environmental sciences proceedings

MDPI

Proceeding Paper

Synoptic Aspects of the Supercell of Halkidiki, 10 July 2019 †

D. Brikas [1,*], P. Siomos [1], I. Nikolaou [2], A. Nikolopoulos [2], D. Papadopoulou-Papaioannou [3] and T. Diomis [4]

[1] Regional Meteorological Center Makedonia of Hellenic National Meteorological Service (HNMS), International Airport Makedonia, 55103 Thessaloniki, Greece; pnsiomos@hotmail.com
[2] Hellenic National Meteorological Service (HNMS), 16777 Hellinikon, Greece; ioanna_emy@hotmail.com (I.N.); alex.nikolop@hotmail.com (A.N.)
[3] Department of Physics, Aristotle University of Thessaloniki, 54124 Thessaloniki, Greece; daphnepapadop@gmail.com
[4] Department of Mathematics, Aristotle University of Thessaloniki, 54124 Thessaloniki, Greece; theodiom@math.auth.gr
* Correspondence: dimibrik@otenet.gr
† Presented at the 16th International Conference on Meteorology, Climatology and Atmospheric Physics—COMECAP 2023, Athens, Greece, 25–29 September 2023.

Abstract: A synoptic study of the supercell of 10 July 2019, Halkidiki, Greece, shows that the gradual approach of a cold front from the north and a short-wave trough from the WSW brought into juxtaposition Saharan and polar air masses, creating a dynamical and thermodynamical environment favourable for severe convection.

Keywords: moist-dry convection; diabatic heating; Saharan air; lid; underrunning; frontogenesis

Citation: Brikas, D.; Siomos, P.; Nikolaou, I.; Nikolopoulos, A.; Papadopoulou-Papaioannou, D.; Diomis, T. Synoptic Aspects of the Supercell of Halkidiki, 10 July 2019. *Environ. Sci. Proc.* **2023**, *26*, 58. https://doi.org/10.3390/environsciproc2023026058

Academic Editors: Konstantinos Moustris and Panagiotis Nastos

Published: 25 August 2023

1. Introduction

Late in the evening of 10 July 2019, a severe supercell thunderstorm affected Central Makedonia, Greece. Maximum wind gusts, reaching nearly 70 kts, were recorded in Halkidiki peninsula, causing ~150 injuries and 7 deaths. Most of the previous work has been carried out on the mesoscale characteristics and some on the predictability of the storm (see [1] and references therein). The supercell initially formed in the South Adriatic Sea, between 09:00 UTC 10 July (hereafter 09Z/10) and 12Z/10 and, continually being re-built, reached the peninsula of Halkidiki at 19Z/10. The aim of this paper is to relate the intense convective event under study to the accompanying synoptic situation. To do this, European Centre for Medium-Range Weather Forecasts (ECMWF) data are interpolated onto isentropic surfaces, as the involved systems are quite baroclinical.

2. Isentropic Chartson θ = 315 Kand Vertical Cross Sections

The main features of interest were already well defined at 18Z/9 (Figure 1a). A polar (Saharan) air mass covered the upper right (lower left) part of the map, with a minimum (maximum) of $p < 300$ hPa ($p > 900$ hPa) in north-eastern Europe (Northwest Africa).

Three main jets could be observed. Associated with anupper-level wave (ULW), an STJ streak, exceeding 46 m/s on the 350 K surface, was located just off the Algerian coast. A**m**id **l**evel**j**et (MLJ) can be seen below the STJ, anticyclonically surrounding the "crest" of the Saharan air mass. The PJ cyclonically surrounded the "base" of the north-eastern European polar air mass, with wind speeds nearly reaching 34 m/s at 315 K. The maximum PJ-associated wind speeds were not captured, as their core was far from both the 315 K and the 350 K surface, located between them, at ~330 K. Numbers in blue (red) font, e.g., 270 (220) at 18Z/9 (Figure 1a), indicate the elevation (hPa) of the 330 (350) K surface in the core of the main PJ (STJ) streaks. The main atmospheric fronts have been drawn, with the aid of isobaric data of wind, temperature and **m**ean **s**ea **l**evel **p**ressure (MSLP, not shown). At MSL, the boundaries of the main air masses were defined by the respective fronts. The

cold front in the north defined the southward boundary of the polar air mass, whereas the two fronts in the south defined the poleward boundary of the Saharan air mass. Higher up, on the 315 K surface, the boundary of the polar (Saharan) air mass was defined by a zone of tight pressure gradient, locally reaching 250 (100) hPa over a distance of 150 km.

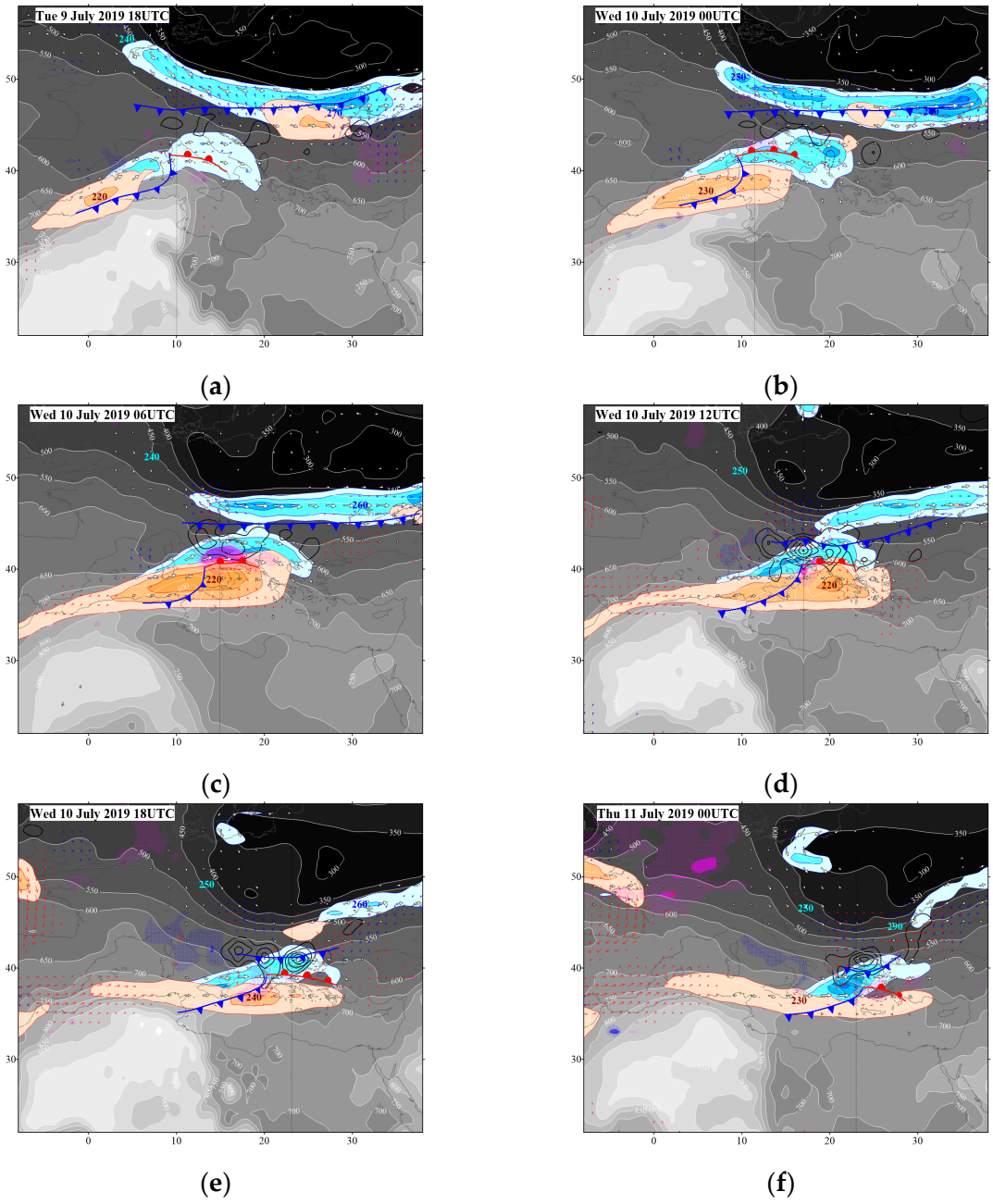

Figure 1. (**a**) For 18Z/9.Background shading and white labelled lines: topography (per 50 hPa) of the θ = 315 K isentropic surface. Areas where $MSLP_t$–$MSLP_{t\text{-}6h}$ is smaller (greater) than −2 (+2) hPa/6h are stippled in purple (blue), with the stippling becoming finer every 1 hPa/6h. Blue (red) isotachs denote 315 (350) K wind speed stronger than 22 (40) m/s, per 4 (5) m/s. Dark (light) shades of blue (orange) cover areas of high (low) wind speed. White thick arrows outlined by a black line are 315 K vectors of wind exceeding 15 m/s. Red (blue) single arrows denote 350 (330) K AG winds exceeding 7 m/s. Areas of diabatic warming (cooling) exceeding 7.5 K/day are enclosed by continuous (dotted) lines. The contour increment is 7.5 K/day. A black dotted straight line is the trace of the respective cross section. (**b**–**f**) As in a, but for the rest of the times in the study period.

The Mediterranean barometric low, associated with the ULW, was located over Corsica, as inferred by the intersection between the associated cold and warm fronts. Nearly all of the diabatic warming (indicative of latent heat release) occurred in the zone between the associated warm front and the primary cold front in the north. This sounds sensible, as the orientation of the warm front implies a southerly low-level current, the veering of which with height implies strong warm (and humid) air advection towards the primary cold front to the north (see Figure 2).

As the STJ and PJ approached each other during the study period (Figure 1b–e), the zone between the two fronts became narrower and the initially scattered areas of weak diabatic warming at 18Z/9 gradually consolidated into intense features that have to be associated with severe convective events. The highest "concentration" of diabatic heating took place during 12–18Z/10 (Figure 1d,e) above the area of Northern Greece (~45 K/day and 38 K/day, respectively), along the track of the supercell under study (see Figure 3.2 of [1]). The STJ-MLJ (PJ) was gradually strengthened by at least 5 m/s due to the amplification of the ULW (southward advance of the polar air mass—see decreasing lat. of 350 hPa isobar), reaching a maximum speed at 06Z/10 (Figure 1c), just before the supercell under study initially appeared, in the area of the South Adriatic. Associated with the above, south-easterly (north-westerly) AG flow across the PJ (STJ) entrance (exit) also picked up and **u**pper **l**evel **d**ivergence (ULD, data not shown) increased as the two jets approached each other to "couple". This favoured moist convection, either directly through the upward motion in the underlying layer, or indirectly through the deepening of the surface low, as ULD is associated with pressure falls. As the ULW and the associated surface low drifted away from the European cold front at the end of the study period (00Z/11, Figure 1f), a weakening occurred of the main fronts/jets/AG currents and also a jet de-coupling, which led to a reduction in ULD and, hence, a weakening of the tropospheric ascent. As shown in the last chart of Figure 1 (panel f), all convection occurring at this time must have been elevated, as it was behind the surface cold front.

Meridional vertical sections are presented in Figures 2 and 3, across the areas of most intense convective activity, essentially along the same meridians as in [1], in order to shed light on the dynamic processes associated with the preconditioning of the synoptic environment to a state favourable for the triggering and maintenance of the supercell. Apart from convective activity, the cross sections were intended to capture as many features of the following as possible: (i) minimum distance between cold and warm front, (ii) thermally direct–indirect ageostrophic vertical circulations and (iii) subtropical (polar) jet exit (entrance) coupling. The main frontal surfaces were drawn with the aid of (i) the temperature (T) advection, $-V\nabla T$, where V is the 2D horizontal wind vector and (ii) entropy, θ, for the vertical distribution of which the reader is referred to [1].

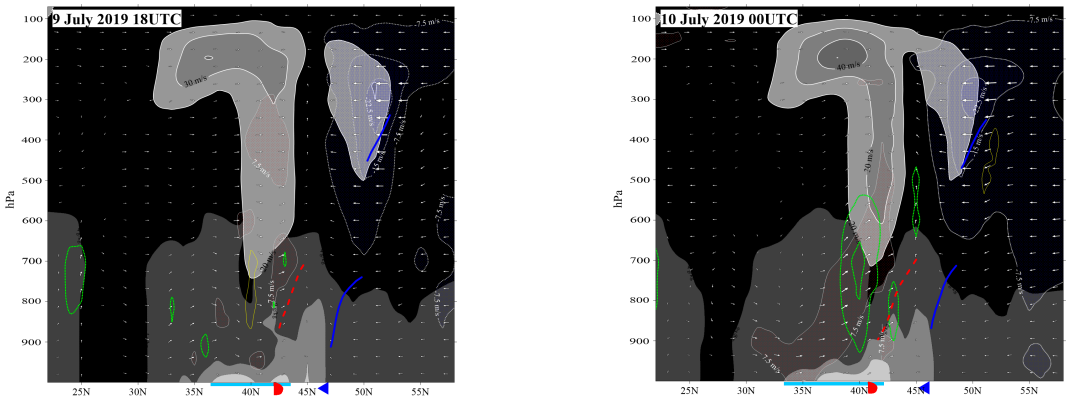

(**a**) (**b**)

Figure 2. *Cont.*

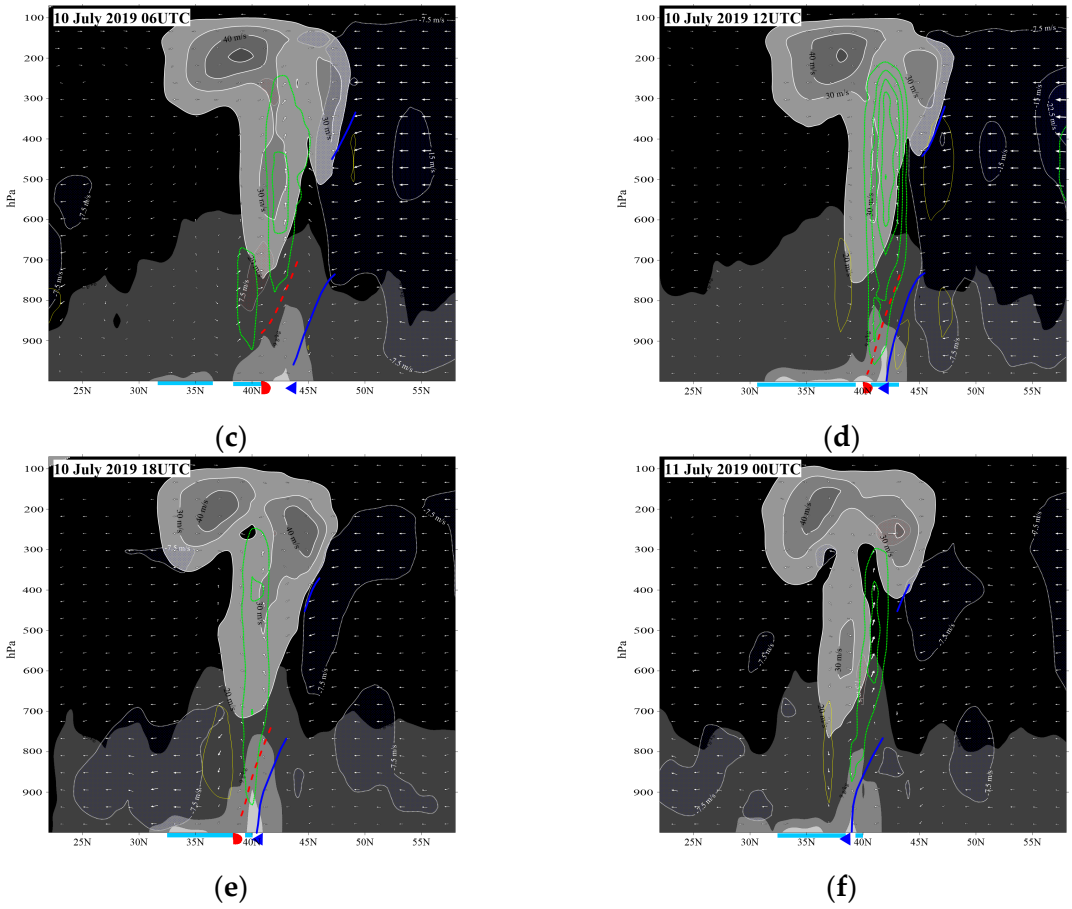

Figure 2. (**a**) Vertical cross section along λ = 10° east 18Z/9. Background shading: specific humidity per 5 g/kg. First isoline is 14 g/kg. Light (dark) shading covers areas of high (low) humidity. Transparent shading with thick white labelled isotachs: zonal wind component (normal to section) > 20 m/s. Dark (light) shading covers areas of high (low) wind speeds. Blue (red) transparent stippling enclosed by dotted (continuous) thin white-labelled isotachs: northerly (southerly) wind component (parallel to section) > 7.5 m/s. White arrows outlined by black line are "hybrid" vectors of vertical circulation: x-comp.: meridional component of wind (parallel to section), y-comp.: vertical motion (ω). Areas of ascent (subsidence) stronger than 0.4 Pa/s, are enclosed by thick dotted green (thin continuous yellow) non-labelled isolines per 0.4 Pa/s. Bottom of figure: surface fronts are indicated by conventional symbols, frontal surfaces by conventionally coloured thick lines and geographical extent of marine areas by a light blue colour. (**b**–**f**) As in a, but for longitudes λ = 11.5, 15, 17, 23 and 23° E, resp., for the rest of the times of the study period.

The background of the sections of Figure 2 (3) is specific humidity (equivalent potential temperature, θ_e). The zonal wind speed and the frontal surfaces are common between Figures 2 and 3. Omega (diabatic heating) is shown in Figure 2 (3) as a measure of convective activity/vertical circulation. Arrows in Figure 2 (3) represent the full (AG) wind vertical circulation. The first meridional cross section (18Z/9) was drawn along 8° E, just ahead of the advancing ULW. The STJ (PJ) cores were at ~37° N (~52° N) and 200 (270) hPa. The cold (warm) front was located at 47° N (43° N) at the surface. A continuous (broken) blue (red) line marked the limit of the cold (warm) air mass in the vertical, to indicate that the associated entropy contrast permitted little (some) mass exchange through it. Both frontal surfaces tilted towards colder air. Southerlies (northerlies) prevailed in the warm (cold) air mass (Figure 2a). Deep large-scale confluence was deduced from the combination of the zonal and meridional wind components, which maximized in the zone between the two surface fronts. This resulted in air parcel (downstream) frontogenesis and the distance between the two fronts gradually reduced (see the whole sequence of cross sections in

both Figures 2 and 3). In agreement with this, the AG vertical circulation had a thermally direct sense (Figure 3a) in the zone between the two fronts, with cold (warm) air subsiding (ascending) behind the cold (warm) frontal surface and northerly (southerly) AG flow prevailing at low (high) levels.

Shallow dry convection was observed in the warm (Saharan) air mass, with up/down areas of $|\omega| > 0.4$ Pa/s (Figure 2a). From the vertical extent of the good mixing of humidity (Figure 2a), θ_e (Figure 3a) and θ itself (data not shown, see [1]), it is gathered that the upward vertical extent of the Saharan air mass was 600–500 hPa. The manifestation in the zonal wind field, of the extension of a well-mixed Saharan air mass up to the mid-troposphere, is the existence of a MLJ at 500 hPa, since a strong negative meridional thermal gradient existed below there and a zero gradient above, even positive, due to adiabatic cooling associated with the intense dry convection in the Saharan air mass. Low down, a near surface layer was observed of high values of humidity (Figure 2a) and θ_e (Figure 3a) as cool and humid marine air masses were trapped below ~950 hPa, under the lid posed by the hot Saharan air masses. The under-running of these humid air masses occurred at the northward edge of the Saharan air mass, as the southerly low-level flow, associated with the deepening low, ahead of the advancing ULW, acted to transport moisture out of the inversion. The level of the isoline of 9 g/kg indeed increased abruptly from 950 hPa behind (to the south of) the warm front (under the Saharan air mass) to 800 hPa ahead (north) of it.

The width of the inter-frontal zone diminished gradually as time went by (see Figure 2b–e) and humid air masses were squeezed in a narrower area, resulting in an increasing water vapour concentration. The level of the 14 g/kg isoline indeed increased from ~950 hPa at 18UTC/9 (Figure 2a) to ~900 hPa 24 h later, at 18Z/10 (Figure 2e). This was the "worst" hour from the humidity viewpoint, as the 9 g/kg isoline also reached its highest level at this time, ascending to 750 hPa over the Gulf of Thermaikos, where the event under study attained its maximum intensity. From the θ_e viewpoint, the θ_e = 345 K isoline reached its highest level, ~820 hPa at 18Z/10, confirming that this time was the most favourable one for severe convection. As the meridional distance between the two fronts reduced, the meridional distance of the convective activity (see diabatic heating in Figure 3) from the MLJ reduced, too, reaching a zero value at 18Z/10. The vectorial sum of the 60 kts of westerly momentum aloft, which was very likely transported downwards in the storm downdrafts, with the ~10 kts of northerly momentum at low levels (Figure 2e), amounted to an~70 kts WNW-erly wind at the surface.

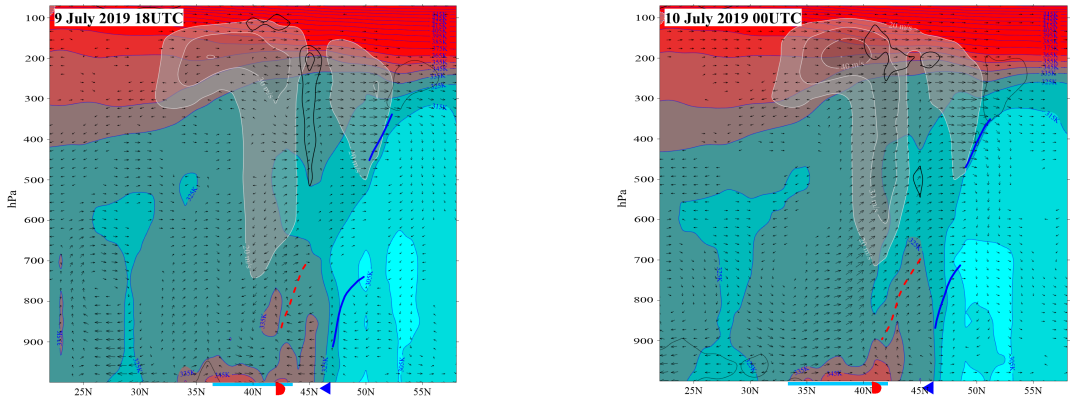

(**a**) (**b**)

Figure 3. *Cont.*

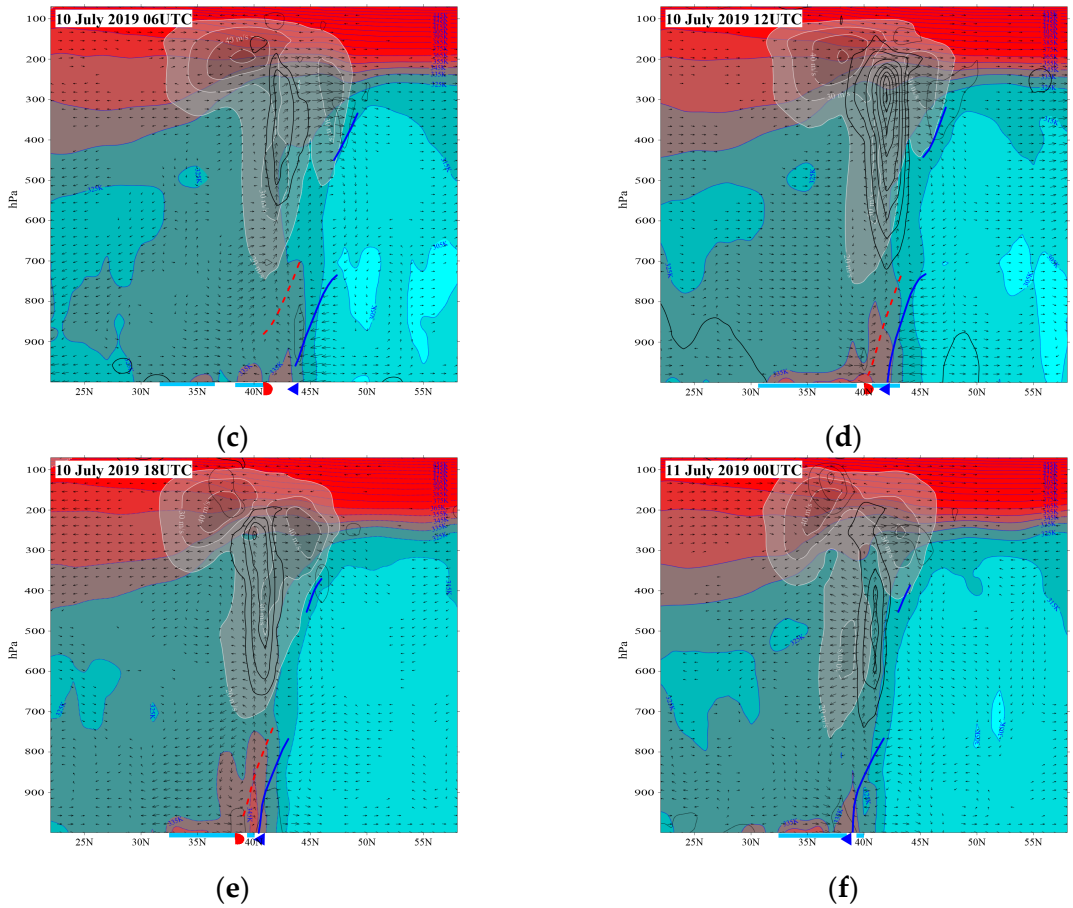

Figure 3. As in Figure 2, but the background coloured field is θ_e (blue-labelled isotherms per 10 K). Red (blue) shading covers areas of high (low) moist entropy. Zonal wind speed is the only field in common with Figure 2. Arrows are as in Figure 2, but for the AG, instead of the full meridional wind component. Areas of diabatic warming (cooling) stronger than 10 K/day are enclosed by thick continuous (thin-dotted) black non-labelled isolines per 10 K/day.

3. Conclusions

A synoptic study of the super-storm of 10 July 2019 has produced with the following results. During the 24 h period that preceded the event, convective activity occurred along the northern Mediterranean coast, in a zonally elongated area between a strong cold front to the north and a warm front to the south. Polar (Saharan) air masses to the north (south) did not particularly favour moist convection, as they were too cold to convect (too hot and posed a lid to low level moisture). Between the two fronts, both thermodynamics and dynamics favoured the breakout of convection. A southerly low-level current was established across the front, promoting under-running. The low-level moisture that exited the Saharan air mass beneath the inversion was free to convect, provided there was a lifting mechanism. A likely one was the STJ and PJ coupling aloft. But an even more efficient lifting factor was the approach of the cold front from the north, which was associated with a thermally direct AG transverse circulation, whose rising branch was located above the inter-frontal zone. The two above mechanisms are inter-related, via the frontogenesis that was promoted by large scale confluence, and which took place in an area that contained the entrance of the inter-frontal zone. Due to the confluence, the two fronts gradually approached one another and so the concentration of moisture increased between them, which led to more convective activity. At 18Z/10, around the time that the supercell affected Halkidiki, the width of the inter-frontal zone had already reached a minimum. This brought the MLJ (60 kts) right into the area of the severe convection. The storm downdrafts assisted

the transport of the westerly momentum downwards, which offers an explanation for the severe surface winds.

Author Contributions: Every author contributed equally to all sectors. All authors have read and agreed to the published version of the manuscript.

Funding: This research received no external funding.

Institutional Review Board Statement: Not applicable.

Informed Consent Statement: Not applicable.

Data Availability Statement: The data presented in this study are available at: www.ecmwf.int.

Conflicts of Interest: The authors declare no conflict of interest.

Reference

1. Angelidou, E.; Feidas, H. A case study of a supercell on the 10th July, 2019 based on satellite data. In Proceedings of the Fifteen Panhellenic Conference of Meteorology, Climatology and Atmospheric Physics, Ioannina, Greece, 26–29 September 2021; pp. 944–948.